Enhanced resolution imaging of ultrathin ZnO layers on Ag(111) by multiple hydrogen molecules in a scanning tunneling microscope junction

Shuyi Liu,[1] Akitoshi Shiotari,[2] Delroy Baugh,[3] Martin Wolf,[1] and Takashi Kumagai[1,4,*]

[1]*Department of Physical Chemistry, Fritz-Haber Institute of the Max-Planck Society, Faradayweg 4-6, 14195 Berlin, Germany*

[2]*Department of Advanced Materials Science, The University of Tokyo, 277-8561 Kashiwa, Japan*

[3]*Department of Chemistry & Biochemistry, University of California, Los Angeles, California 90095-1569, USA*

[4]*JST-PRESTO, 4-1-8 Honcho, Kawaguchi, Saitama 332-0012, Japan*

(Received 2 February 2018; revised manuscript received 9 March 2018; published 11 May 2018)

Molecular hydrogen in a scanning tunneling microscope (STM) junction has been found to enhance the lateral spatial resolution of the STM imaging, referred to as scanning tunneling hydrogen microscopy (STHM). Here we report atomic resolution imaging of 2- and 3-monolayer (ML) thick ZnO layers epitaxially grown on Ag(111) using STHM. The enhanced resolution can be obtained at a relatively large tip to surface distance and resolves a more defective structure exhibiting dislocation defects for 3-ML-thick ZnO than for 2 ML. In order to elucidate the enhanced imaging mechanism, the electric and mechanical properties of the hydrogen molecular junction (HMJ) are investigated by a combination of STM and atomic force microscopy. It is found that the HMJ shows multiple kinklike features in the tip to surface distance dependence of the conductance and frequency shift curves, which are absent in a hydrogen-free junction. Based on a simple modeling, we propose that the junction contains several hydrogen molecules and sequential squeezing of the molecules out of the junction results in the kinklike features in the conductance and frequency shift curves. The model also qualitatively reproduces the enhanced resolution image of the ZnO films.

DOI: 10.1103/PhysRevB.97.195417

Ultrahigh resolution imaging using functionalized tips of a scanning tunneling microscope (STM) and an atomic force microscope (AFM) has attracted increasing attention as a powerful method to resolve submolecular structures of adsorbates [1]. Carbon monoxide is one of the most common molecules to functionalize the tip apex, which leads to the enhanced spatial resolution in STM [2] and AFM [3–5] and also molecular orbital imaging [6]. It has been found that molecular hydrogen (H_2) weakly bound in an STM junction can also enhance the spatial resolution and resolve submolecular structures of planar organic molecules, introducing the idea of scanning tunneling "hydrogen" microscopy (STHM) [7]. The enhanced resolution with H_2 has been explained by Pauli repulsion in the junction [8–10]. However, it was reported that the enhanced resolution also occurs at a relatively large tip to surface distance where the Pauli repulsion is negligible [11]. A theoretical study has proposed that the enhanced resolution results from the change of the adsorption state of the trapped H_2 in the junction [12]. Hydrogen molecular junctions (HMJs) have also been studied as a simple model of molecular junctions, and conductivity and mechanical properties of the HMJs have been measured using mechanical break junction [13–17], STM [18–20], and AFM experiments [21]. However, the accurate structure of HMJs, which is directly associated with the enhanced resolution imaging mechanism of STHM, has remained poorly understood.

So far, the enhanced resolution imaging of STHM has been used to observe planar organic molecules in most cases, but it will be a useful method to obtain ultrahigh resolution images of extended two-dimensional structures on surfaces. Ultrathin oxide films serve as a unique model, for instance, to study the atomistic structure and elementary processes of catalysis using surface science approaches [22–24]. The highly reproducible and controlled preparation of the oxide films also allow to examine intrinsic defects which should have a crucial impact on their properties. For instance, it has been known that oxygen vacancies commonly occur in ZnO [25]. Additionally, line defects may also significantly affect physical properties of low-dimensional materials as simulated for a ZnO sheet [26]. In order to assess the local defects, ultrahigh resolution imaging is a powerful tool.

The experiments were performed in an ultrahigh vacuum (UHV) chamber equipped with a low-temperature STM/AFM (ScientaOmicron GmbH) operated with a Nanonis SPM controller. All measurements were performed at 5 K. Simultaneous STM/AFM measurements were conducted using a tuning fork sensor with an electrochemically etched W tip. The sensor showed a resonance frequency at ∼23 221 Hz with a quality factor of 20 000–40 000 at 5 K. For the pure STM measurements, a chemically etched PtIr or Au tip was used. The Ag(111) surface was cleaned by repeated cycles of argon ion sputtering and annealing up to 670 K. The ultrathin ZnO layers were grown on a Ag(111) surface using the reactive deposition method described elsewhere [27,28]. To deposit molecular hydrogen, the surface was exposed to a pure H_2 gas (background pressure of $\sim 5 \times 10^{-8}$ mbar) in the SPM stage at ∼14 K. A Naphthalocyanine (NPc) molecule was deposited from a Knudsen cell (∼700 K) onto the surface at room temperature.

*kuma@fhi-berlin.mpg.de

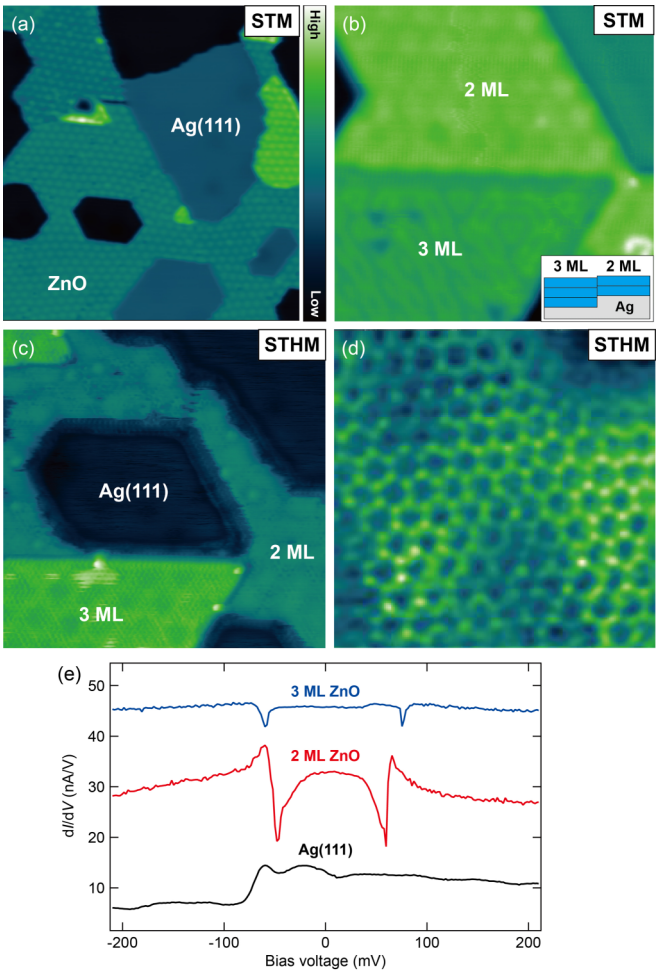

FIG. 1. (a) Overview STM image of ultrathin ZnO layers epitaxially grown on Ag(111) (5 K, $V_s = 1$ V, $I_t = 0.1$ nA, 120×70 nm^2), showing both bare Ag(111) surface and ZnO layers. (b) STM image scanned at a low bias voltage (5 K, $V_s = 0.1$ V, $I_t = 0.1$ nA, 0.2×0.2 nm^2). The 3-ML ZnO layer is formed at a lower Ag terrace so that the apparent height is slightly lower than the 2-ML ZnO, as illustrated in the inset. (c) STHM image after dosing 22 L H_2. (5 K, $V_s = 0.1$ V, $I_t = 0.1$ nA, 0.2×0.2 nm^2) (d) The enlarged STHM images of 2-ML ZnO layers scanned with the constant height mode. The images are obtained by a PtIr tip. (e) dI/dV spectra measured over Ag(111), 2-ML and 3-ML ZnO with the same tip after dosing H_2 gas. The tip (PtIr) height was fixed at 1 V and 1 nA.

Figure 1(a) shows an overview STM image of the ZnO film on the Ag(111) surface. The ZnO layer exhibits a moiré pattern resulting from the ZnO(0001)-(7 × 7)/Ag(111)-(8 × 8) coincidence structure [28], which is less pronounced at a low bias voltage [Fig. 1(b)]. The thickness of the ZnO layer can be identified by measuring the conduction band minimum with scanning tunneling spectroscopy (STS) because it varies depending on the thickness [28,29]. The ZnO surface is not terminated by hydrogen as verified by infrared vibrational spectroscopy [30]. Figure 1(c) displays an STM image after exposing the surface to a 22 Langmuir (1 L = 1×10^{-6} Torr s) H_2 gas, which does not affect the surface morphology. However, the presence of H_2 in the junction leads to the enhanced resolution of the ZnO layers [Fig. 1(d)]. We found that scanning in the constant height mode allows more stable imaging than the constant current mode. The lattice constant of ∼0.32 nm determined from the high resolution image is consistent with the previous SXRD measurement (0.3303(2) nm [31]). However, we could not distinguish the Zn or O atoms even in the high resolution image.

H_2 adsorbs preferentially on the ZnO layers at a relatively low exposure (∼10 L) of the surface to a H_2 gas. However, as the exposure is increased, H_2 also adsorbs on the Ag(111) surface (see Fig. S1 of the Supplemental Material [32]). Although the H_2 molecules on the ZnO layers are not clearly visible in the STM image, the existence of H_2 in the junction is manifested as characteristic dips in the conductance spectra [Fig. 1(f)]. Similar nonlinear current-voltage characteristics have been observed in HMJs. This feature results from the bistable motion of the H_2 molecule trapped in the junction, which is driven by vibrational excitation [18,33–35].

We found that the high resolution image of the ZnO layer can be obtained at a specific tip to surface distance and this range is relatively narrow. Figure 2(a) shows the conductance to tip displacement curves $G(z)$ measured over 2-ML ZnO with and without H_2. In contrast to the monotonic increase of $G(z)$ over the bare ZnO layer, three kinklike features are observed for the HMJ (marked by the red arrows in Fig. 2(a). Figures 2(b)–2(f) display the topographic images of 2-ML ZnO obtained at different gap distances. The highest resolution is observed at a relatively large tip to surface distance [Fig. 2(c)] at which the kinklike feature appears in the $G(z)$ curve [marked by the open circle in Fig. 2(a)]. A similar behavior is observed for different tip materials, namely W, PtIr, and Au, and the distance between the kinks ($\Delta d_{\mathrm{kink}} \approx 0.3$ nm) was not affected by apex conditions (see Fig. S2 of the Supplemental Material [32]).

We also imaged NPc molecules on the ZnO layer by STHM [Fig. 3(a)]. Figure 3(b) displays the enhanced resolution image of the ZnO layer and the NPc molecules obtained in the constant height mode. This image enables us to find the adsorption geometry of the molecules [a schematic model of the ZnO layer is superimposed in Fig. 3(a)]. As mentioned above, although the Zn or O atom cannot be directly identified, here we speculate it from the adsorption geometry of the molecules. The N atoms may prefer to interact with cation atoms in a dielectric layer. For instance, it was shown that free-base phthalocyanine adsorbs on an NaCl layer with the imine N atoms bonded to the Na atoms [36]. Accordingly, we tentatively suggest that the imine N atoms of NPc interact with the Zn atoms and the adsorption geometry as shown in Fig. 3(c). The high resolution image of NPc [Fig. 3(b)] is similar to the previous STHM image of organic molecules in which the atom positions appear dark [8]. In contrast, the atom positions of the ZnO layers appear as a bright spot [Fig. 1(d)].

In order to gain further insight into the imaging mechanism with the HMJ, we investigated the mechanical properties of the junction over the NPc and ZnO layer using AFM. Figure 3(d) shows the $\Delta f(z)$ curve measured over a 2-ML ZnO and NPc molecule in the presence of H_2. The tunneling current $I(z)$ was also recorded simultaneously with a bias voltage of 10 mV applied. The $\Delta f(z)$ curve exhibits a kinklike feature [as indicated by arrows in Fig. 3(d)] which also occurs in the $I(z)$ curves at the same tip to surface distance. The kinks should

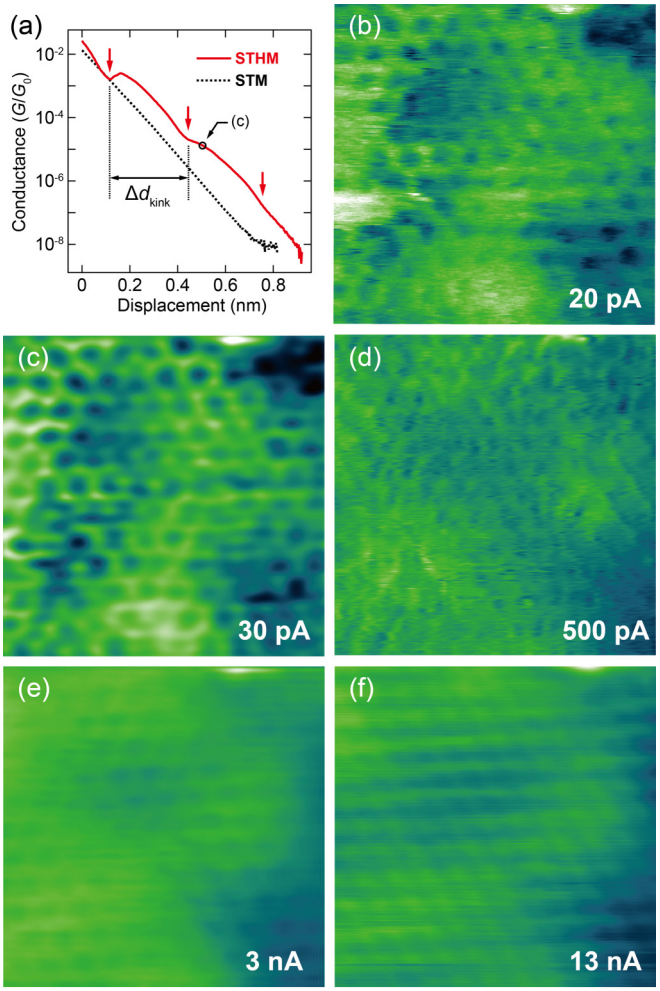

FIG. 2. (a) Conductance–tip displacement curves measured over 2-ML ZnO before and after dosing H_2. G_0 is the quantum of conductance. The zero point in the horizontal axis corresponds to the tip height with set points of $V_s = 30$ mV, $I_t = 30$ nA and $V_s = 30$ mV, $I_t = 60$ nA for the STM and STHM junction, respectively. The arrows indicate kinklike features. (b–f) STM images of 2-ML ZnO scanned in the presence of H_2 and obtained at four different tip to sample distances that are determined by the set current as indicated in the figures (5 K, $V_s = 30$ mV, 3.5×3.5 nm^2). The conductance curve and STM images are obtained with a PtIr tip in a pure STM setup.

result from a structural change inside the junction which causes the change in the conductance and force simultaneously [8]. The $\Delta f(z)$ measured over an NPc molecule shows a repulsion interaction at the gap distances where the enhanced resolution can be obtained [the orange area in Fig. 3(d)]. Therefore, Pauli repulsion is responsible for the enhanced resolution as reported previously [8,9]. However, the enhanced resolution over the ZnO layer is observed in the attractive force regime where Pauli repulsion is negligible, suggesting a different imaging mechanism.

We found that the STHM imaging for the ZnO layer is not affected by the bias voltage. Similar results can be obtained at a bias voltage either above or below the dip energy in the dI/dV spectra [Fig. 1(e)]. Above the dip voltage, a rotational or vibrational mode of H_2 in the junction should be excited. Also,

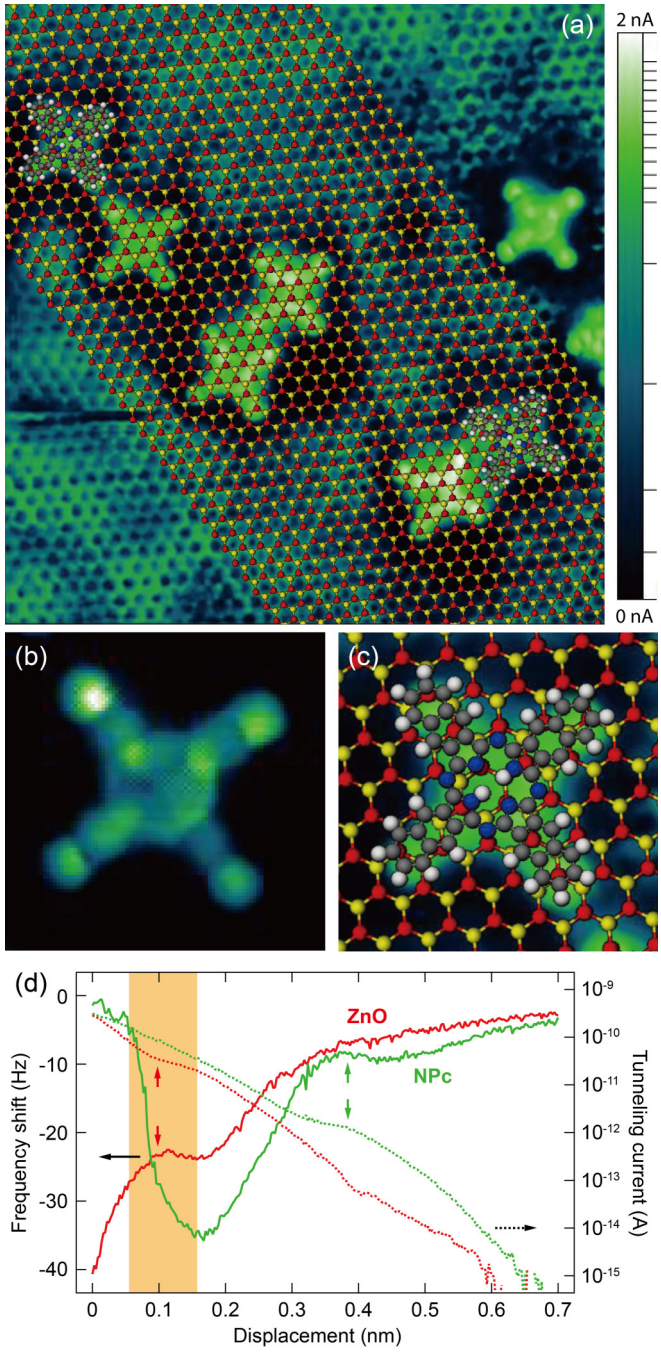

FIG. 3. (a) STHM image of 2-ML ZnO and NPc molecules obtained in the constant height mode (5 K, $V_s = 50$ mV, 11×11 nm^2). The image is obtained with a PtIr tip in a pure STM mode. The structure model of the ZnO and NPc molecules is superimposed (red: Zn; yellow: oxygen). (b) Enlarged STHM image (constant height mode) of NPc molecule. (c) Enlarged structure model of NPc. (d) $\Delta f(z)$ (solid lines) and $I(z)$ (dashed lines) recorded simultaneously over 2-ML ZnO (red curves) and NPc molecule (green curves) under the same tip conditions. The data are obtained with a W tip in the qPlus configuration. A small bias voltage of $V_s = 10$ mV is applied during the measuring. The arrows mark the kinklike features in the $I(z)$ and $\Delta f(z)$ curve. The orange region indicates the gap distance where the enhanced resolution of both ZnO layer and NPc molecule were obtained simultaneously with the constant height mode.

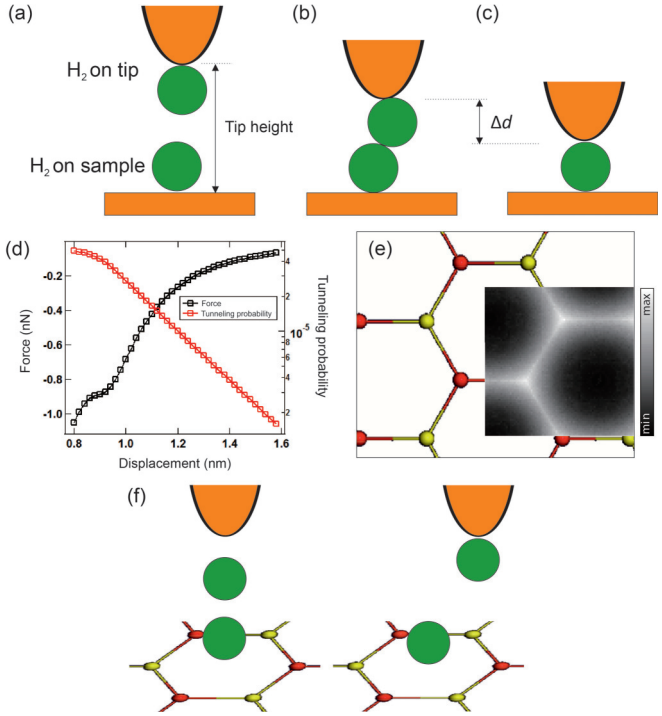

FIG. 4. (a–c) Schematic model of the HMJ with two H_2 molecules at different tip heights. (d) Simulated vertical force (perpendicular to the ZnO surface) and the total tunneling probability (T) as a function of the tip height (gap distance) from the surface. The tip is located above the Zn-O bond. (e) Simulated STHM image (T_1 map) of the ZnO film in the constant height mode at a tip height of 0.93 nm. The simulated image is superposed on the ZnO structure. (f) Schematic of the HMJ when placing the tip over the hollow or the Zn (or O) atom positions. The H_2 on the tip is closer to the apex when the tip is located over the atom positions.

the same behaviors are observed for different tip materials (W, PtIr, and Au) and under different tip conditions which may result in a slightly different adsorption geometry of the H_2 molecule on the tip. Therefore, the orientation of the trapped H_2 molecules may play a minor role.

In order to gain qualitative insight into the imaging mechanism as well as an emergence of the kinklike features in the $I(z)$ and $\Delta f(z)$ curves, we considered a simple model in which two H_2 molecules are trapped inside the junction as shown in Fig. 4(a); one molecule is adsorbed on the ZnO surface and the other is attached to the tip apex. When the STM junction becomes small, one of the molecules is expected to be squeezed outside the junction, leading to the kinklike feature in the $I(z)$ and $\Delta f(z)$ curves. A second kink is then expected when the other H_2 molecule is squeezed out. The gap distance difference (Δd) between Figs. 4(b) and 4(c) is estimated to be about 0.3 nm from the equilibrium distance between H_2 molecules [37], which should correspond to Δd_{kink} of ~0.3 nm found in Fig. 2(a). It is worth noting that a similar kinklike feature in the conductance curve was observed for the STM junction containing one or two Xe atom(s), which shows a larger Δd_{kink} (~0.45 nm) in the latter case [38].

Based on the above model, we simulated the conductance and force curves as demonstrated in Ref. [9]. A pairwise Lennard-Jones (LJ) potential is employed to describe the interaction of the tip-H_2-ZnO junction. The ZnO layer is modeled by the h-BN-like single-layer sheet using the lattice parameters obtained from the experiment. The H_2 molecule is represented by a single spherical atom, and the tip is a single atom. The conductance is described by approximating the tunneling probability $T \propto T_1 T_2 T_3$, where T_1, T_2, and T_3 are the tunneling probability of the tip-H_2, H_2-H_2, and H_2-ZnO gaps, respectively (see Fig. S3 of the Supplemental Material [32]). These tunneling probabilities decay exponentially as the gap distance (d_n) increases, $T_n \propto \exp(-\beta_n d_n)$, where β_n corresponds to the decay constant ($n = 1, 2, 3$). β_n is determined by the tunneling barrier, but the precise barrier shape cannot be obtained either by the model or experiment and we fix $\beta_n = 1\,\text{Å}^{-1}$. The simulation reproduces the kinklike feature in the $I(z)$ and $\Delta f(z)$ curves observed in the experiment [Fig. 4(d)]. We find that the relaxation of two H_2 molecules gives rise to the kink in the tunneling probability and force curves at the tip height around 0.9 nm. This distance corresponds to the sum of each equilibrium distance (tip-H_2, H_2-H_2, and H_2-ZnO). It should be noted that the kink position is not affected by the value of β_n and is determined solely by the interactions within the junction. The kink appears when the interactions start to displace the H_2 molecules.

We also simulated the STHM image at the gap distance around the kinklike feature in the calculated tunneling probability and force curves, where the enhanced resolution is expected in the experiment (Fig. 2). It is found that the two-dimensional mapping of T_1 and T_3 shows a similar contrast and the atom positions of the ZnO film appear as a protrusion, which is consistent with the experiment [Fig. 4(e): T_1 map]. However, the T_2 map exhibits the opposite contrast to T_1 and T_3 and the hollow site appears as a protrusion with a periodicity of 0.55 nm (see Fig. S4 of the Supplemental Material [32]), thus being inconsistent with the experiment. This result may suggest that T_1 and/or T_3 dominates the total tunneling probability and the image contrast of the STHM. The total tunneling probability, thus the simulated STHM image, is sensitive to the value of β_n. As mentioned above, we set $\beta_n = 1\,\text{Å}^{-1}$ but this assumption is unlikely since the barrier shape for each process (T_1, T_2, T_3) should be considerably different. Due to the interaction between H_2 and the tip (or surface) the tunneling barrier may be narrower than that between two H_2 molecules, which makes T_1 and T_3 much more sensitive to displacement of the H_2 molecule than T_2. Additionally, H_2 molecules may cover the ZnO surface and the electron tunneling would occur between the H_2 on the tip apex with multiple H_2 on the ZnO surface and suppress the contrast of T_2.

The contrast of the T_n map is explained by displacement of the H_2 molecules in the junction. The model finds that H_2 prefers to weakly adsorb to the hollow site of the ZnO layer. This adsorption geometry is similar to H_2 on graphene [39,40]. If H_2 is located at the hollow site, the distance between two H_2 molecules becomes larger at the atom positions of ZnO [Fig. 4(f)]. This would weaken the attractive interaction between two H_2 molecules. As a result, the H_2 molecule on the tip moves toward the tip apex, leading to the increase of the tunneling probability between them through the reduction of the barrier (brighter feature at the atom positions than the

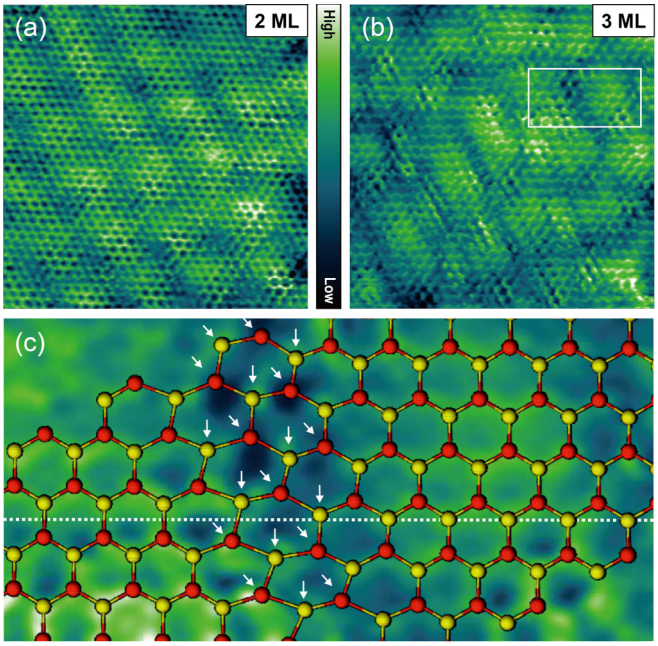

FIG. 5. (a–b) Constant current STHM images of 2-ML (5 K, $V_s = 0.05$ V, $I_t = 0.05$ nA, 10×10 nm^2) and 3-ML (5 K, $V_s = 0.03$ V, $I_t = 0.03$ nA, 10×10 nm^2) ZnO layer. The images are obtained with a PtIr tip in a pure STM setup. (c) Enlarged STHM image of 3-ML ZnO marked with a white box in (b). The proposed structure model is superimposed on the image. The dashed line is a guide to the eye for the lattice displacement. The white arrows indicate the disordered atom positions.

hollow site). At the tip height around the kink, the relaxation of two H_2 molecules occurs during scanning, which modifies the tunneling probability and eventually leads to the enhanced resolution. However, when one of the H_2 molecules is squeezed outside the junction at a smaller tip to surface distance, the enhancement effect disappears. On the other hand, at a large tip to surface distance (far away from the kink position), the intermolecular interaction is too weak to induce the relaxation of two H_2 molecules; thus no enhanced resolution is expected. It should be noted that the experimental image [Fig. 1(d)] is not as sharp as the simulated result. Additionally, the simulated force curves at different tip positions show clear site dependence (see Fig. S5 of the Supplemental Material [32]), which is, however, also not observed in the experiment. These differences should be acceptable for our simplified model.

Using STHM we resolve a more defective structure for 3-ML ZnO layers than for 2 ML. As compared in Figs. 5(a) and 5(b), the 2-ML ZnO layer shows more uniform (ordered) structure than 3 ML. As shown in the enlarged STHM image [Fig. 5(c)], dislocation defects are frequently observed for the 3-ML ZnO layer where the lattice displacement of ~0.8 Å occurs and distorted honeycomb structures may be involved [marked by arrows in Fig. 5(c)]. Dislocation of ZnO thin films could result from the strain due to the lattice mismatch with the substrate [41]. However, having considerably fewer dislocation defects in 2-ML ZnO rules out this possibility. A previous study suggests that the structural change from an h-BN-like flat layer to a wurtzitelike structure may occur in the 2- and 3-ML ZnO [29,42]. We tentatively assign the dislocation area to the structural change from the flat structure to the corrugated surface of the wurtzitelike structure.

In summary, we applied STHM to obtain the enhanced resolution image of the 2- and 3-ML ZnO layers on Ag(111). The electric and mechanical properties of the HMJ were investigated by a combination of STM and AFM. It was found that the enhanced resolution is obtained at a relatively large and specific tip to surface distance. In the HMJ, the gap-distance-dependent conductance and frequency shift curves show kinklike features, which are absent in a hydrogen-free junction. Based on a simple modeling of the HMJ, we propose that the junction contains several H_2 molecules and the kinklike features in the conductance and frequency shift curves can be explained by squeezing H_2 molecules outside the junction. Using STHM we resolved a more defective structure of 3-ML ZnO than of 2 ML, possibly caused by the partial structural transition from a planar h-BN-like layer to a wurtzitelike structure. Our results demonstrate that STHM will be a powerful tool to image two-dimensional extended structures with ultrahigh resolution.

T.K. acknowledges the support by JST-PRESTO (JPMJPR16S6). T.K. and M.W. acknowledge the support by the Deutsche Forschungsgemeinschaft through Sfb951. A.S. acknowledges the support by JSPS KAKENHI Grant No. JP17K19024.

[1] P. Jelínek, J. Phys.: Condens. Matter **29**, 343002 (2017).
[2] C.-l. Chiang, C. Xu, Z. Han, and W. Ho, Science **344**, 885 (2014).
[3] L. Gross, F. Mohn, N. Moll, P. Liljeroth, and G. Meyer, Science **325**, 1110 (2009).
[4] A. Shiotari and Y. Sugimoto, Nat. Commun. **8**, 14313 (2017).
[5] J. Peng, J. Guo, P. Hapala, D.n. Cao, R. Ma, B. Cheng, L. Xu, M. Ondráček, P. Jelínek, E. Wang, and Y. Jiang, Nat. Commun. **9**, 122 (2018).
[6] L. Gross, N. Moll, F. Mohn, A. Curioni, G. Meyer, F. Hanke, and M. Persson, Phys. Rev. Lett. **107**, 086101 (2011).
[7] R. Temirov, S. Soubatch, O. Neucheva, A. C. Lassise, and F. S. Tautz, New J. Phys. **10**, 053012 (2008).
[8] C. Wagner and R. Temirov, Prog. Surf. Sci. **90**, 194 (2015).
[9] P. Hapala, G. Kichin, C. Wagner, F. S. Tautz, R. Temirov, and P. Jelínek, Phys. Rev. B **90**, 085421 (2014).
[10] O. Krejci, P. Hapala, M. Ondracek, and P. Jelinek, Phys. Rev. B **95**, 045407 (2017).
[11] A. Yu, S. Li, G. Czap, and W. Ho, J. Phys. Chem. C **119**, 14737 (2015).
[12] H. Wang, S. Li, H. He, A. Yu, F. Toledo, Z. Han, W. Ho, and R. Wu, J. Phys. Chem. Lett. **6**, 3453 (2015).
[13] R. H. M. Smit, Y. Noat, C. Untiedt, N. D. Lang, M. C. van Hemert, and J. M. van Ruitenbeek, Nature **419**, 906 (2002).
[14] M. Kiguchi, R. Stadler, I. S. Kristensen, D. Djukic, and J. M. van Ruitenbeek, Phys. Rev. Lett. **98**, 146802 (2007).

[15] Sz. Csonka, A. Halbritter, G. Mihály, O. I. Shklyarevskii, S. Speller, and H. van Kempen, Phys. Rev. Lett. **93**, 016802 (2004).
[16] T. Nakazumi, S. Kaneko, and M. Kiguchi, J. Phys. Chem. C **118**, 7489 (2014).
[17] Y. Li, S. Kaneko, S. Fujii, and M. Kiguchi, J. Phys. Chem. C **119**, 19143 (2015).
[18] J. A. Gupta, C. P. Lutz, A. J. Heinrich, and D. M. Eigler, Phys. Rev. B **71**, 115416 (2005).
[19] S. Li, A. Yu, F. Toledo, Z. Han, H. Wang, H. Y. He, R. Wu, and W. Ho, Phys. Rev. Lett. **111**, 146102 (2013).
[20] F. D. Natterer, F. Patthey, and H. Brune, ACS Nano **8**, 7099 (2014).
[21] C. Lotze, M. Corso, K. J. Franke, F. von Oppen, and J. I. Pascual, Science **338**, 779 (2012).
[22] H.-J. Freund and G. Pacchioni, Chem. Soc. Rev. **37**, 2224 (2008).
[23] S. Shaikhutdinov and H.-J. Freund, Annu. Rev. Phys. Chem. **63**, 619 (2012).
[24] H.-J. Freund, J. Am. Chem. Soc. **138**, 8985 (2016).
[25] H. Morkoç and Ü. Özgür, *Zinc Oxide: Fundamentals, Materials and Device Technology* (Wiley, New York, 2009).
[26] N. Lu, H.Y. Guo, W. Hu, X. J. Wu, and X. C. Zeng, J. Mater. Chem. C **5**, 3121 (2017).
[27] Q. Pan, B. H. Liu, M. E. McBriarty, Y. Martynova, I. M. N. Groot, S. Wang, M. J. Bedzyk, S. Shaikhutdinov, and H.-J. Freund, Catal. Lett. **144**, 648 (2014).
[28] A. Shiotari, B. H. Liu, S. Jaekel, L. Grill, S. Shaikhutdinov, H.-J. Freund, M. Wolf, and T. Kumagai, J. Phys. Chem. C **118**, 27428 (2014).
[29] T. Kumagai, S. Liu, A. Shiotari, D. Baugh, S. Shaikhutdinov, and M. Wolf, J. Phys.: Condens. Matter **28**, 494003 (2016).
[30] B.-H. Liu, J. A. Boscoboinik, Y. Cui, S. Shaikhutdinov, and H.-J. Freund, J. Phys. Chem. C **119**, 7842 (2015).
[31] C. Tusche, H. L. Meyerheim, and J. Kirschner, Phys. Rev. Lett. **99**, 026102 (2007).
[32] See Supplemental Material at http://link.aps.org/supplemental/10.1103/PhysRevB.97.195417 for additional experimental data and simulation results.
[33] W. H. A. Thijssen, D. Djukic, A. F. Otte, R. H. Bremmer, and J. M. van Ruitenbeek, Phys. Rev. Lett. **97**, 226806 (2006).
[34] A. Halbritter, P. Makk, Sz. Csonka, and G. Mihály, Phys. Rev. B **77**, 075402 (2008).
[35] M. L. Trouwborst, E. H. Huisman, S. J. van der Molen, and B. J. van Wees, Phys. Rev. B **80**, 081407(R) (2009).
[36] K. Miwa, H. Imada, S. Kawahara, and Y. Kim, Phys. Rev. B **93**, 165419 (2016).
[37] M. Oobatake and T. Ooi, Prog. Theor. Phys. **48**, 2132 (1972).
[38] A. Yazdani, D. M. Eigler, and N. D. Lang, Science **272**, 1921 (1996).
[39] D. Henwood and J. D. Carey, Phys. Rev. B **75**, 245413 (2007).
[40] P. T. Lam, P. V. Dung, A. Sugiyama, N. D. Duc, T. Shimoda, A. Fujiwara, and D. H. Chi, Comput. Mater. Sci. **49**, S15 (2010).
[41] U. Ozgur, Y. I. Alivov, C. Liu, A. Take, M. A. Reshchikov, S. Doğan, V. Avrutin, S. J. Cho, and H. Morkoc, J. Appl. Phys. **98**, 041301 (2005).
[42] I. Demiroglu and S. T. Bromley, J. Phys.: Condens. Matter **28**, 224007 (2016).